DOI: 10.13009/EUCASS2019-183

Study of a Hydro-Pneumatic Buffer with a Variable Damper for Launch Vehicle Landing Legs

Hongpeng Ma, Shoujun Zhao*, Zongxia Jiao***
**Beijing Institute of Precision Mechatronics and Controls, Beijing 100076, China*
***School of Automation Science and Electrical Engineering, Beihang University, Beijing 100191, China*
mhp_bit@163.com, shoujunzhao@vip.sina.com, zxjiao@buaa.edu.cn

Abstract
A hydro-pneumatic buffer with a variable damper for launch vehicle landing legs was proposed. The mathematical model for dynamics was built to analyze its performances. Results show, for a vertical landing vehicle with 25000kg and 3m/s, the buffer shows competent. The micro-scale flow simulation indicated a good uniformity of the flow field and an ideal cushion effect. Compared with a fixed damper, the maximum resistance is 22% lower and the cushion efficiency 2% higher. The buffer can tolerate a landing speed as high as 5m/s, providing a promising option for reusable vertical landing launch vehicles.

Nomenclature

m_r Mass of the landing vehicle
m_n Mass of the inner cylinder
m_h Mass of the spool valve
x Displacement of the inner cylinder
x_h Displacement of the spool valve
k Stiffness coefficient of the spring
x_0 Pre-compressed length of the spring
l_{a0} Initial length of the gas chamber
l_3 Length of the spool valve damping holes
l_4 Length of the one-way valve damping holes
l_5 Length of the inner cylinder damping holes
l_{h0} Initial length of the annular chamber
l_h Length of the annular chamber
V_a Volume of gas chamber
P_a Pressure of the gas chamber
P_1 Pressure of the upper oil chamber
P_2 Pressure of the lower oil chamber
P_n Pressure of the inner chamber
A_a Action area of the P_a on the inner cylinder
A_1 Downward action area of the P_1
A_{11} Upward action area of the P_n
A_n Downward action area of the P_n
A_2 Upward action area of the P_2
A_{xd} Action area of the P_1 on the spool valve
A_{dd} Action area of the P_n on the spool valve
A_t Action area of the F_t on the spool valve
F_{fn} Sliding friction of the inner cylinder
F_{fh} Sliding friction of the spool valve
F_{zn} Damping force of the inner cylinder
F_{zh} Damping force of the spool valve
F_t Spring force
n_1 Number of the spool valve damping holes
n_2 Number of the inner cylinder damping holes
d Inner diameter of inner cylinder
d_1 Inner diameter of outer cylinder
d_2 Diameter of annular chamber
d_{21} Diameter of flow hole
d_3 Diameter of spool valve damping holes
d_4 Diameter of one-way valve damping hole
d_5 Diameter of inner cylinder damping holes
d_6 Small end diameter of annular chamber
d_7 Large end diameter of annular chamber
d_{xd} Diameter of the upper end of spool valve
v_0 Initial impact velocity of the landing vehicle

DOI: 10.13009/EUCASS2019-183

1. Introduction

In recent years, all major space nations are developing reusable launch vehicles to reduce the cost of entering space. SpaceX as the first company to achieve successful vertical recoveries is on the road of reducing the launching price by about 20% [1-2].
The cushioning performances of landing legs are directly related to the integrity of the landing rockets [3-4]. So far, the aluminum honeycomb buffers were successfully used in the Falcon 9 and some other planetary landing vehicles. However, since the honeycombs must to be crushed, the legs must be disassembled and refurbished after each landing. Therefore, the retractable landing legs and hydraulic buffers have been tested in Falcon series [5].
With applications in aircrafts and ground vehicles as a learning basis [6-11], a new designed variable damping hydro-pneumatic buffer was put forward, the impact dynamics calculation and the micro-scale flow simulation were showed in this study.

2. Structure of the buffer

The schematic diagram of the hydro-pneumatic buffer is shown in Figure 1, composed of an inner cylinder, an outer cylinder, a foot, seals, etc. The inner cylinder has a gas chamber, a floating piston, an upper oil chamber, an annular chamber, a spool valve, two preload springs, and a one-way damping valve. The floating piston isolates the gas chamber from the upper oil chamber. The outer cylinder has a lower oil chamber and seals.

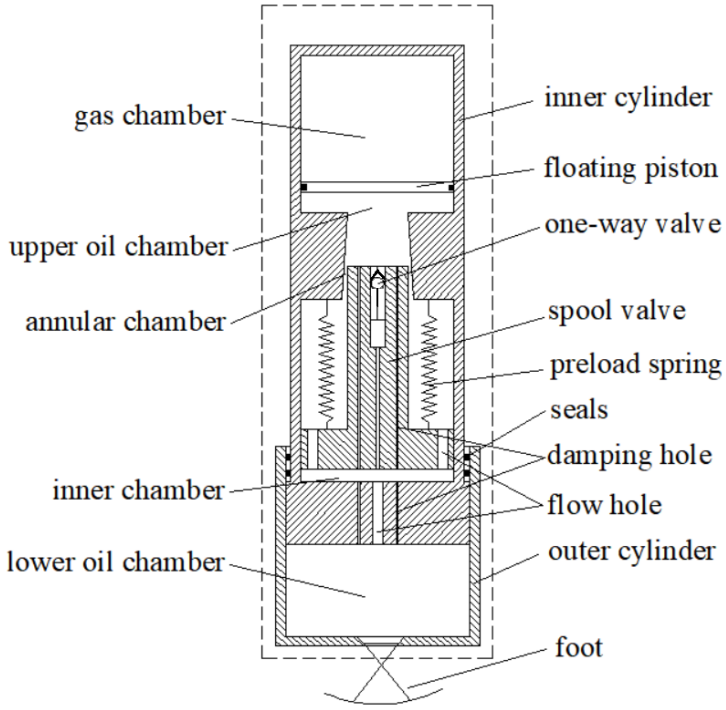

Figure 1: Hydro-pneumatic buffer schematic diagram

The buffer operates in 2 phases: the compression stroke and the recovery stroke.
During the compression stroke, the inner cylinder moves downward under the landing impact, with the pressure of the lower oil chamber increasing. The spool valve is pushed upwards when the oil enters the upper oil chamber through the damping holes, the gas chamber is compressed by the moving floating piston. In this phase, the impact energy is converted into the thermal energy of the oil and the compression energy of the enclosed gas.
During the recovery stroke, the floating piston is pushed downward by the compressed gas and the oil returns into the lower oil chamber. In the end, the pressure of each chamber is balanced by the weight of the landed launch vehicle.
It operates with a one-way valve to realize only one compression stroke, eliminating the unexpected bumping effects, and with an annular damping passage tapering during the compressing stroke, to ensure a better cushion effect.

DOI: 10.13009/EUCASS2019-183

3. Dynamics calculation

3.1 Mathematical model

3.1.1 Motion differential equation

During the landing buffering of the launch vehicle, the force analysis of the inner cylinder and the spool valve are performed respectively, as shown in Figure 2.

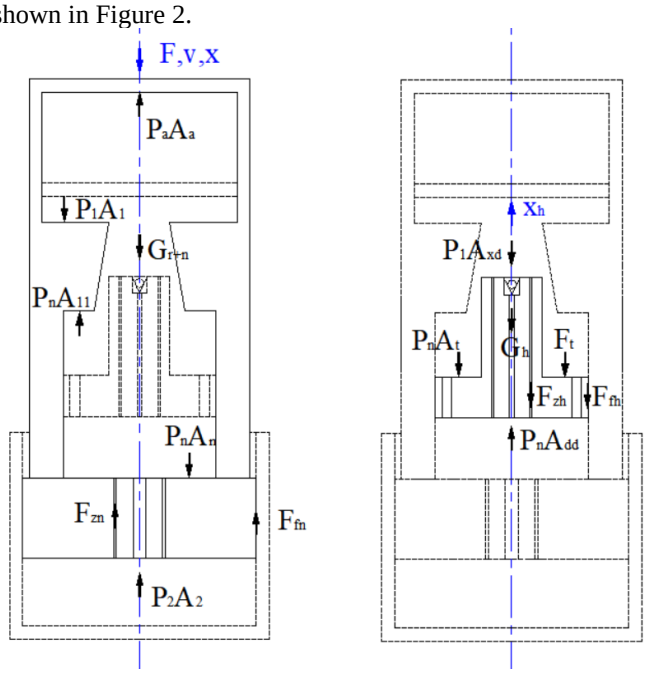

a) Inner cylinder b) Spool valve

Figure 2: Force analysis

It can be considered that P_a=P_1 because of the negligible mass of the floating piston, and the friction of the system is negligible. According to Newton's second law, the differential equations are as follows:

$$\begin{cases} (m_r + m_n)\dfrac{d^2x}{dt^2} = (m_r + m_n)g + P_a(A_1 - A_a) + P_n(A_n - A_{11}) - F_{zn} - P_2A_2 \\ m_h\dfrac{d^2x_h}{dt^2} = -m_hg - P_aA_{xd} + P_n(A_{dd} - A_t) - F_t - F_{zh} \end{cases} \quad \textbf{(1)}$$

Where $\mathbf{g} = 9.80665\ \mathrm{m\cdot s^{-2}}$.

3.1.2 Damping force equation

The damping force of the inner cylinder contains two parts: 1) F_{zn1}, generated by the damping holes of the inner cylinder; 2) F_{zn2}, generated by the annular chamber. The formula can be obtained [12]:

$$F_{zn} = F_{zn1} + F_{zn2} = 8n_3\pi\mu l_5 v_3 + 8\pi\mu l_h v_4 \quad \textbf{(2)}$$

Where v_3, v_4 are the average velocity of the oil in the holes.
The damping force of the spool valve contains three parts: 1) F_{zh1}, generated by the damping hole of the spool valve; 2) F_{zh2}, generated by the annular chamber; 3) F_{zh3}, generated by the damping hole of the one-way valve.
When the buffer is in the compression stroke, the one-way valve is closed, so the calculation equation is as follows:

$$F_{zh} = F_{zh1} + F_{zh2} = 8n_1\pi\mu l_3 v_5 + 8\pi\mu l_h v_6 \quad \textbf{(3)}$$

DOI: 10.13009/EUCASS2019-183

Where v_5, v_6 are the average velocity of the oil in the holes.
When the buffer is in the recovery stroke, the one-way valve is opened, so the calculation equation is as follows:

$$F_{zh} = F_{zh1} + F_{zh2} + F_{zh3} = 8n_1\pi\mu l_3 v_7 + 8\pi\mu l_h v_8 + 8\pi\mu l_4 v_9 \quad \textbf{(4)}$$

Where v_7, v_8, v_9 are the average velocity of the oil in the holes.

3.1.3 Flow equation

1) Compression stroke flow equation
During the compression stroke, the one-way valve in the middle of the spool valve is closed, and the oil flows from the lower oil chamber into the upper oil chamber through these holes shown in Figure 3.

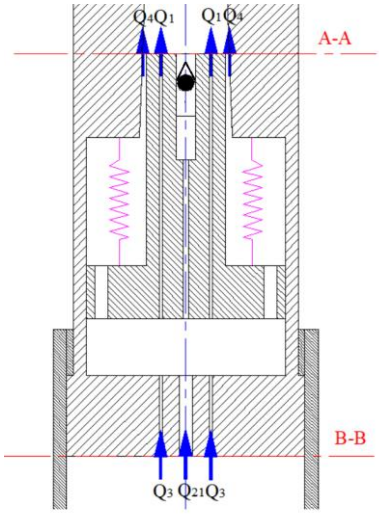

Figure 3: Flow analysis (Compression stroke)

According to the law of conservation of mass, for sections A-A and B-B, it can be concluded that:

$$Q_3 + Q_{21} = Q_4 + Q_1 \quad \textbf{(5)}$$

2) Recovery stroke flow equation
During the recovery stroke, the one-way valve is opened, and the oil flows from the upper oil chamber into the lower oil chamber, as shown in Figure 4.

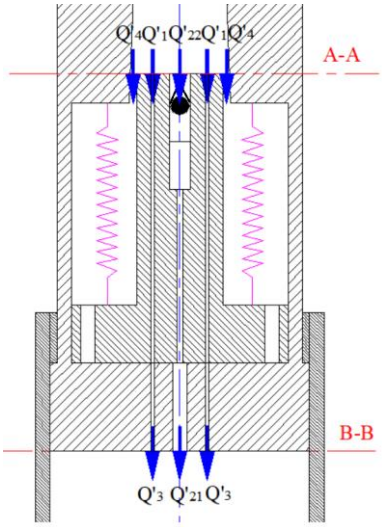

Figure 4: Flow analysis (Recovery stroke)

DOI: 10.13009/EUCASS2019-183

According to the law of conservation of mass, for sections A-A and B-B, there is as follows:

$$Q_1' + Q_{22}' + Q_4' = Q_3' + Q_{21}' \tag{6}$$

Since the damping holes are all elongated holes, the pressure loss is mainly represented by the loss along the path, and the oil flowing in the elongated holes is generally laminar. Therefore, the flow of the elongated holes can be calculated by the following formula [11]:

$$Q = \frac{\pi D^4}{128\mu l}\Delta P \tag{7}$$

Where D is the diameter of the damping hole; l is the length of the damping hole; ΔP is the pressure difference between the damping hole.

3.1.4 Ideal gas law

The inert gas selected for the gas chamber is high-purity nitrogen, and the ideal gas law equation is:

$$P_a V_a^n = P_0 V_0^n \tag{8}$$

Where n is the gas multivariable index, n can be selected as 1.35 because of the experience [13].

3.1.5 Dynamics equations

The impact dynamics equations of the buffer are as follows:

$$\begin{cases} (m_r + m_n)\dfrac{d^2x}{dt^2} = (m_r + m_n)g + P_a(A_1 - A_a) + P_n(A_n - A_{11}) - F_{zn} - P_2A_2 \\ m_h\dfrac{d^2x_h}{dt^2} = -m_hg - P_aA_{xd} + P_n(A_{dd} - A_t) - F_t - F_{zh} \\ Q_3 + Q_{21} = Q_4 + Q_1, \quad \text{When compression stroke} \\ Q_1' + Q_{22}' + Q_4' = Q_3' + Q_{21}', \quad \text{When recovery stroke} \\ P_a = P_0\left(\dfrac{V_0}{V_a}\right)^{1.35} \end{cases} \tag{9}$$

The supplementary equations are:

$$\begin{cases} Q_1 = Q_1' = n_1\dfrac{\pi d_3^{\,4}}{128\mu l_3}(P_n - P_1) \\ Q_{21} = Q_{21}' = n_2\dfrac{\pi d_{21}^{\,4}}{128\mu l_5}(P_2 - P_n) \\ Q_3 = Q_3' = n_3\dfrac{\pi d_5^{\,4}}{128\mu l_5}(P_2 - P_n) \\ Q_4 = Q_4' = \dfrac{\pi d_2(P_n - P_1)}{12\mu(l_{h0} + x_h)}\left(\dfrac{d_2 - d_{xd}}{2}\right)^3 + \dfrac{\pi d_2 v_{xd}}{2}\dfrac{(d_2 - d_{xd})}{2} \\ Q_{22}' = \dfrac{\pi d_{22}^{\,4}}{128\mu l_6}(P_n' - P_1') \\ F_{zn} = 8n_3\pi\mu l_5 v_3 + 8\pi\mu l_h v_4 \\ F_{zh} = 8n_1\pi\mu l_3 v_5 + 8\pi\mu l_h v_6, \quad \text{When compression stroke} \\ F_{zh} = 8n_1\pi\mu l_3 v_7 + 8\pi\mu l_h v_8 + 8\pi\mu l_4 v_9, \quad \text{When recovery stroke} \\ F_t = k(x_0 + x_h) \\ V_a = A_a(l_{a0} - x) \end{cases} \tag{10}$$

The fourth-order Runge-Kutta method is used to calculate the second-order differential equations [14].

DOI: 10.13009/EUCASS2019-183

3.2 Assumptions and inputs

To simplify the calculation, the dynamics simulation model of the buffer is assumed as follows:
(1) The whole buffering process is adiabatic;
(2) There is no oil leakage between the system components;
(3) The gravitation of the oil and other undescribed components are not considered;
(4) The P_a is equal to the P_1;
(5) The viscous oil is incompressible.
This calculation uses Matlab to write the program, the simulation step is 0.001 s, and the time is 2 s. The basic input parameters are shown in Table 1 below.

Table 1: Input parameters

Parameter	Value	Parameter	Value
m_r	25000 (kg)	μ	0.031 (Pa·s)
m_n	40 (kg)	d	0.15 (m)
m_h	10 (kg)	d_1	0.18 (m)
v_0	3 (m/s)	d_6	0.08 (m)
P_a (t=0)	2 (MPa)	d_7	0.12 (m)
ρ	890 (kg/m3)	d_{xd}	0.06 (m)

3.3 Results analysis

Figure 5 is the displacement and velocity of the inner cylinder of the buffer.

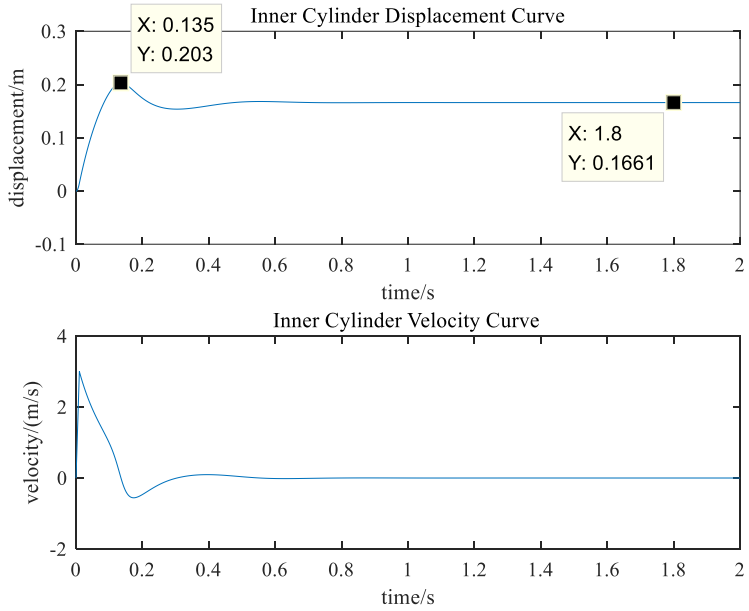

Figure 5: The displacement and velocity curve of the inner cylinder

Figure 5 shows that the displacement of the inner cylinder reaches the maximum value of 0.203 m at t=0.135 s. At the same time, the compression stroke of the buffering ends. At t=0.3~0.6 s, the displacement tends to stabilize at 0.1661 m after a small shock. The initial velocity of the inner cylinder rapidly increases to 3 m/s with the landing impact. Then, the velocity is gradually reduced to 0 m/s.

DOI: 10.13009/EUCASS2019-183

Figure 6 is the displacement and velocity curve of the spool valve.

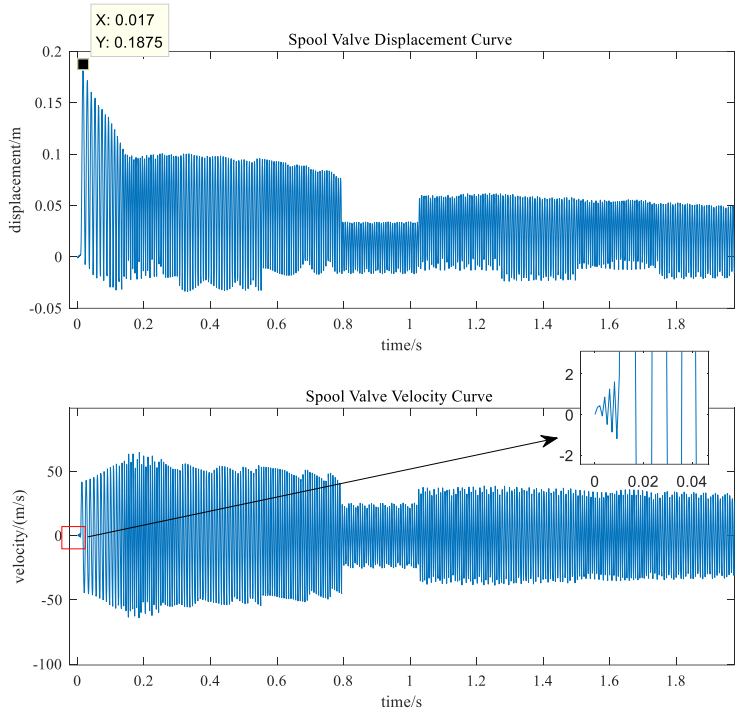

Figure 6: The displacement and velocity curve of the spool valve

Figure 6 shows that the displacement of the spool valve reaches the maximum of 0.1875 m at t=0.017 s. At the beginning, the velocity of the spool valve quickly reaches about 40 m/s after a series of rapid shocks. The maximum velocity is about 50 m/s. After t=0.8 s, the amplitudes of displacement and velocity are reduced significantly.
Figure 7 is the resistant force-time curve.

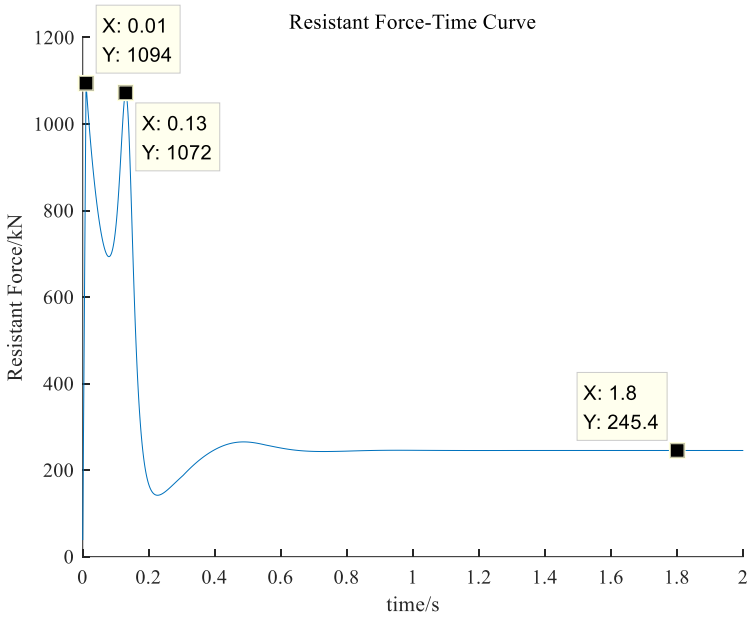

Figure 7: The resistant force-time curve

As shown in Figure 7, the maximum value of the resistant force is 1094 kN, which occurs at t=0.01 s of the moment of landing. At t=0.01~0.13 s, the resistant force quickly reduced to 1072 kN after a rapid drop and up, which corresponds to the compression stroke of the inner cylinder. When t>1 s, the resistant force is stable at 245.4 kN.
Figure 8 is the pressure-time graph of each chamber of the buffer.

DOI: 10.13009/EUCASS2019-183

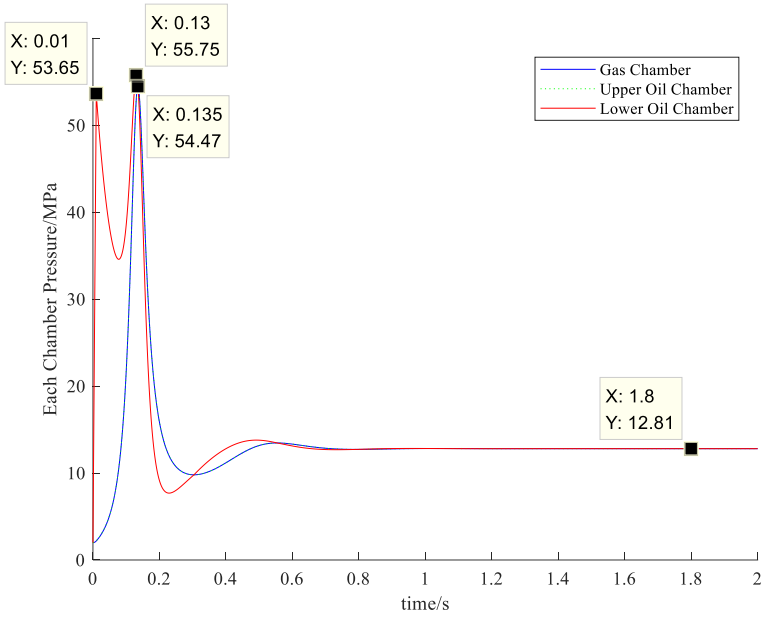

Figure 8: The pressure-time graph of each chamber

Figure 8 shows that the pressure of the lower oil chamber reaches the maximum value of 53.65 MPa instantaneously, then rapidly drops and increases to 55.75 MPa. The pressure of upper oil chamber and gas chamber reached their maximum value of 54.47 MPa at t=0.135 s. Subsequently, all chamber pressure decreased rapidly, and stabilized to 12.81 MPa.

Figure 9 is the graph of resistant force-inner cylinder displacement. As shown in Figure 9, the resistant force has two peak values. The shape of the curve is approximate to the ideal buffer curve.

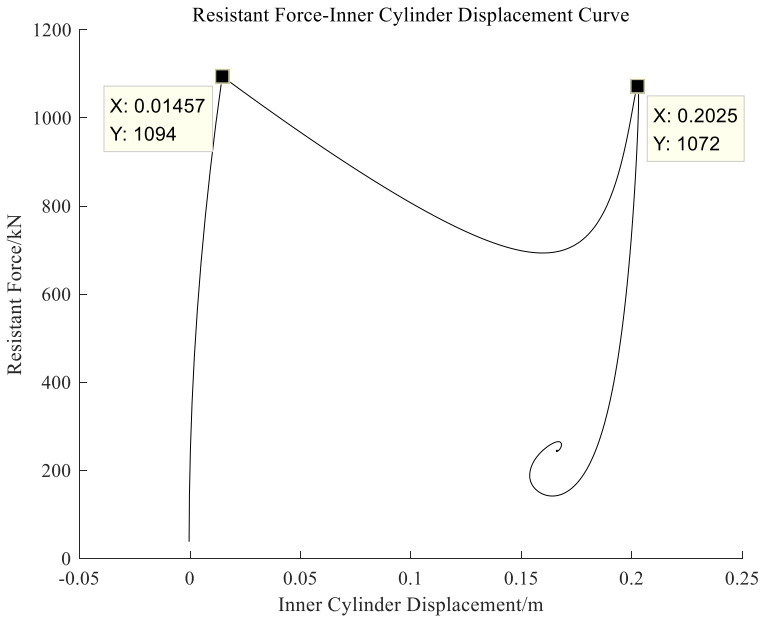

Figure 9: The resistant force-inner cylinder displacement curve

After calculation, the maximum acceleration overload is 4.4 **g** and the buffering efficiency η=82.95%. Therefore, the buffer has better dynamic characteristics and efficiency.

DOI: 10.13009/EUCASS2019-183

4. Flow dynamics simulation

A two-dimensional micro-scale transient flow numerical model of a one-way damping valve was established by using dynamic grid and UDF technique, the micrometer-scale flow field rheological parameters were obtained. All other setup details are described in another paper [15], only the simulation results are given below.
When t=0.135 s, the operating condition of the buffer is the worst, and the inner cylinder reaches the maximum compression displacement. As is shown in Figure 10, the instantaneous pressure peak of the lower oil chamber is approximately 54 MPa.

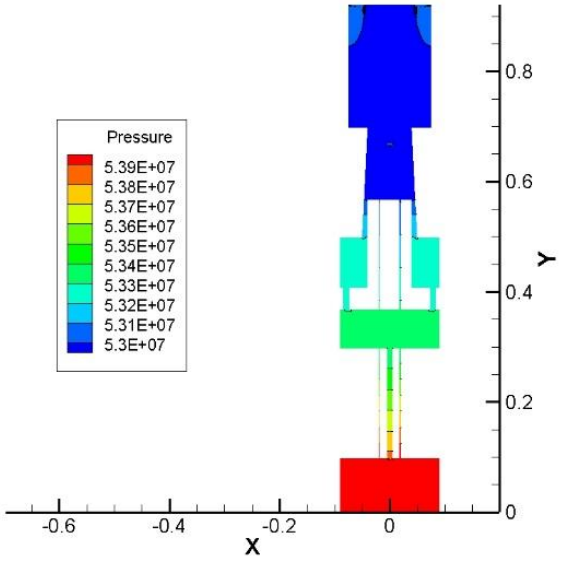

Figure 10: Pressure nephogram (t=0.135 s)

5. Comparisons and prospects

Table 2 shows the comparison results between variable damper structure and conventional fixed damper structures at a landing speed of 3 m/s.

Table 2: Comparison results

	Variable Damper	**Conventional (d_6=d_7=0.1 mm)**	**Conventional (d_6=d_7=0.12 mm)**
Maximum Resistance/(kN)	1094.30	1404.50	1404.50
Cushion Efficiency/(%)	82.95	81.24	81.23

Compared with conventional fixed damper structures, the variable damper structure has a better performance, the maximum resistance is 22% lower and the cushion efficiency 2% higher. Since the resistance force is linear with the landing acceleration overload, the lower the resistance, the smaller the acceleration overload, the smaller the impact on the launch vehicle.
For the landing speed of 5m/s, the oil chamber pressure curve and the overload acceleration curve are calculated respectively. As seen in Figure 11 and Figure 12, the maximum pressure of the two oil chambers are both about 100 MPa, the maximum acceleration overload is about 10 **g**. Therefore, the variable damping hydro-pneumatic buffer can tolerate a landing speed as high as 5 m/s.

DOI: 10.13009/EUCASS2019-183

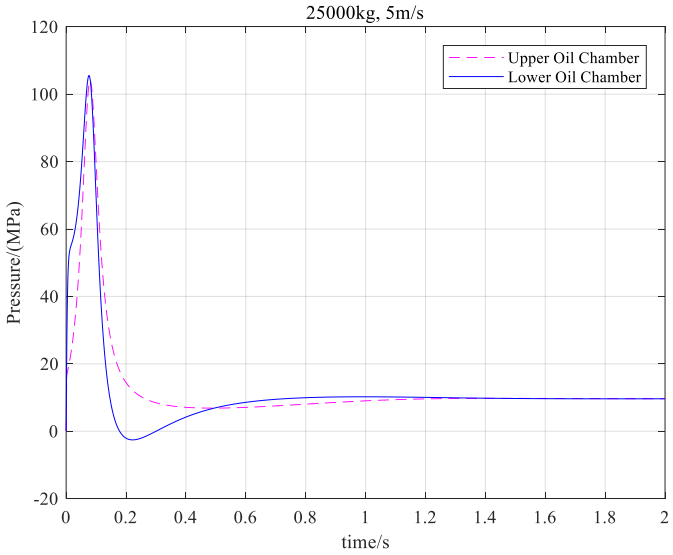

Figure 11: Oil Chamber Pressure (25000kg,5m/s)

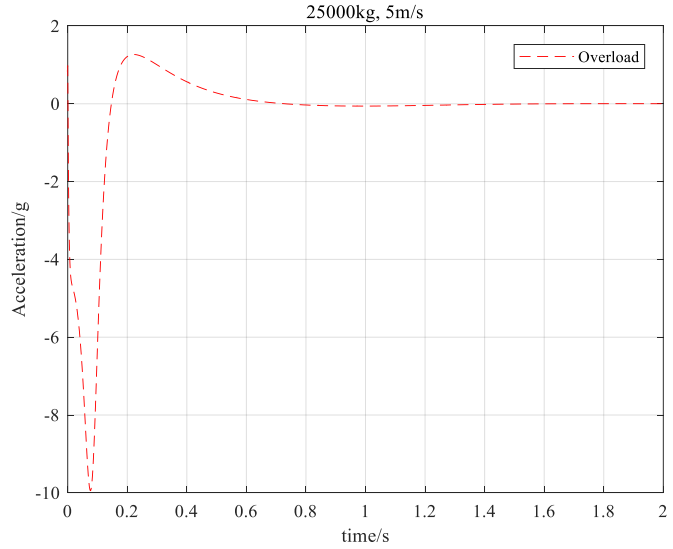

Figure 12: Acceleration overload (25000kg,5m/s)

6. Conclusion

Through the calculation of the variable damping hydro-pneumatic buffer and the comparison with the conventional buffers, the following conclusions can be given:

(1) At a general landing velocity of 3 m/s, the maximum compression displacement of the inner cylinder is 0.203 m, and the maximal pressure of the gas chamber is about 55 MPa. Moreover, the maximal resistant force is 1094 kN, and the buffering efficiency is about 82.95%.

(2) The instantaneous pressure peak of the oil chamber calculated by Fluent is about 54 MPa, which is not much different from the dynamics.

(3) Compared to the conventional hydro-pneumatic buffer, the new buffer has a lower resistance and a lower acceleration overload at an acceptable buffering efficiency, so that the landing impact of the launch vehicle is smaller.

(4) The variable damping hydro-pneumatic buffer can tolerate a landing speed as high as 5m/s, providing a promising option for reusable vertical landing launch vehicles.

DOI: 10.13009/EUCASS2019-183

References

[1] Xiong Zhen, et al. Survey and Review on Development of Falcon 9 Reusable Rocket[J]. Missiles and Space Vehicles, 2016.

[2] Baylor, Michael. "With Block 5, SpaceX to increase launch cadence and lower prices". NASASpaceFlight.com. Retrieved May 24, 2018.

[3] Lu Yu, et al. Progress and Prospect of Reusable Launch Vehicle Technology[J]. Missiles and Space Vehicles, 2017(5):1-7.

[4] Davis L A. First stage recovery[J]. Engineering, 2016, 2(2): 152-153.

[5] Boyle, Alan. "SpaceX's Elon Musk geeks out over Mars interplanetary transport plan on Reddit". GeekWire. Retrieved 24 June 2017.

[6] Sutoh M, Wakabayashi S, Hoshino T. Landing Behavior Analysis of Lunar Probe Based on Drop Tests and RFT in a Vacuum[J]. IEEE Robotics & Automation Letters, 2017, PP(99):1-1.

[7] Xiao J, Zhang M, Yue S, et al. Design and analysis on new landing support of vertical takeoff/landing launch vehicle[J]. Machine Design & Manufacturing Engineering, 2017.

[8] Currey N S. Aircraft landing gear design: principles and practices[M]. American Institute of Aeronautics and Astronautics, 1988.

[9] Pu Zhiming, Wei Xiaohui. Damping Performance Analysis of Fixed Orifice Buffer Landing Gear [J]. System Simulation Technology, 2014, 10(2):125-129.

[10] Huang Hong. Research on Principle and Characteristics of Pneumatic Buffer and Hydraulic Buffer [D]. Zhejiang University, 2003.

[11] Xu T, Liang M, Li C, et al. Design and analysis of a shock absorber with variable moment of inertia for passive vehicle suspensions[J]. Journal of Sound & Vibration, 2015, 355:66-85.

[12] Dong Jixian, etc. Fluid Power Transmission and Control[M]. National Defense Industry Press, 2010.

[13] Lu Yuxiang. Hydraulic and Pneumatic Technical Manual[M]. Mechanical Industry Press, 2002.

[14] Kroese D P, Chan J C C. Matlab Primer[M]// Statistical Modeling and Computation. 2014.

[15] Hongpeng Ma, Shoujun Zhao. The Micro-Scale Flow Simulation of a Hydro-Pneumatic Buffer for Launch Vehicle Landing Legs[C]// International Conference on Fluid Power & Mechatronics. 2019.